JOURNAL OF CATALYSIS 137, 186–198 (1992)

Deuterium Tracing Studies and Microkinetic Analysis of Ethylene Hydrogenation over Platinum

SCOTT A. GODDARD,[1] RANDY D. CORTRIGHT, AND J. A. DUMESIC[2]

Department of Chemical Engineering, University of Wisconsin, Madison, Wisconsin 53706

Received February 3, 1992; revised March 23, 1992

Deuterium tracing experiments of ethylene hydrogenation over platinum were conducted at temperatures from 248 to 333 K and D_2/C_2H_4 pressure ratios between 50:75 and 150:25 Torr. Information about the rates of adsorption/desorption and hydrogenation processes on the surface was extracted by kinetic analysis of the deuterium tracing data combined with results from steady-state kinetic studies and temperature programmed desorption experiments. This analysis suggests that the essential surface chemistry can be described by a Horiuti–Polanyi mechanism that includes competitive and noncompetitive hydrogen adsorption pathways, each modified by a hydrogen activation step. The importance in these analyses of utilizing data from diverse experimental measurements is illustrated.

INTRODUCTION

The quantification of heterogeneous catalytic reaction kinetics is an important aspect of research to probe the essential surface chemistry of catalytic processes. Importantly, a quantitative description of the reaction kinetics in terms of fundamental surface chemical processes can be used to consolidate diverse experimental data for the purpose of predicting catalyst performance over a wide range of reaction conditions. A well-known difficulty in this approach is that kinetic data of a given type alone are not generally sufficient to establish a thorough description of the surface chemistry. In this respect, we have reported elsewhere that microkinetic analysis of diverse experimental data from such techniques as steady-state kinetic studies, isotopic tracing, and temperature programmed desorption provides a detailed description of the essential surface chemistry involved in ethylene hydrogenation over platinum (*1*). In the present paper, we focus attention on that portion of the microkinetic analysis dealing with data from isotopic tracing.

The use of isotopic tracing to elucidate reaction pathways over heterogeneous catalysts is well established, e.g., Ref. (*2*). Previous investigations have interpreted the results of deuterium tracing experiments of ethylene hydrogenation in terms of relative rates of elementary steps. For example, Kemball (*3*) showed that the deuterium distributions in ethylene and ethane may be used to derive the relative rates of elementary steps for the Horiuti–Polanyi associative mechanism (*4*), without specifying the slow steps. Sato and Miyahara (*5*) evaluated the rates of elementary steps for the Horiuti–Polanyi associative mechanism from the results of ethylene deuteration over a Pt film. They concluded that the desorption of ethane was irreversible and that the first hydrogenation of adsorbed ethylene was faster than the other steps.

In the present paper we amplify the use of isotopic tracing by showing the utility of analyzing in a unified fashion the results of isotopic tracing with data from steady-state kinetic studies collected over a wide range

[1] Present address: Amoco Research Center, Naperville, IL 60563.

[2] To whom correspondence should be addressed.

0021-9517/92 $5.00

of reaction conditions, as well as with results from temperature programmed desorption studies at ultra-high vacuum conditions. The approach of this paper for ethylene hydrogenation is an extension of that described by Happel for the water–gas shift and methanation reactions (*6*). In short, the deuterium tracing studies provide information about the relative rates of elementary steps, steady-state kinetic studies provide information on the rate-limiting or slow steps, and temperature programmed desorption studies provide information about adsorption/desorption processes. The kinetic information extracted from combined analyses of these diverse data is, in general, more detailed and reliable than conclusions reached from analysis of any particular set of data alone.

In a previous study, we reported the results of steady-state kinetic studies of ethylene hydrogenation on platinum over a wide range of reaction conditions (*7*). This steady-state study showed that the hydrogen kinetic order decreases continuously from unity at 336 K to half-order as the temperature is decreased below 248 K. An ethylene kinetic order of zero was observed at ethylene pressures above 75 Torr, whereas the ethylene kinetic order was negative below this pressure. Analyses of the steady-state kinetic results suggested that at the lower temperatures, the reaction takes place on sites where hydrogen and ethylene adsorption do not compete, whereas competitive adsorption of these species takes place at higher temperatures and lower ethylene pressures. The combined analyses of results from these steady-state kinetic studies with selected data from isotopic tracing suggested that a hydrogen activation step is required for both the competitively and noncompetitively adsorbed hydrogen (*1*). In the present study, we explore these conclusions further by analysis of data from isotopic tracing of ethylene hydrogenation over platinum, collected over the same wide range of reaction conditions employed in our steady-state kinetic studies.

EXPERIMENTAL

Deuterium tracing experiments were conducted in a glass system operated as a flow-through, differential reactor. A schematic diagram of the experimental apparatus is shown in Fig. 1. Reactant gases were treated to remove possible impurities such as water and oxygen. Helium (Liquid Carbonic) was purified by passage through copper turnings at 473 K, followed by molecular sieves (13X) at 77 K. Ethylene (Matheson, 99.5%) was treated by passage through a molecular sieve trap at 195 K. Hydrogen (Liquid Carbonic) and deuterium (Matheson, 99.5%) were treated by passage through a Deoxo unit (Engelhard) and a bed of molecular sieves (13X) at 77 K.

The reactor was made of glass (16-mm OD), upstream of which was a glass coil that facilitated temperature equilibration of the reactant gases. Different reaction temperatures were obtained by immersing the reactor into a well-mixed water bath. The lowest reaction temperature of 248 K was obtained by using a well-stirred 65% ethylene glycol/water bath that was cooled by the combination of a Flexi-Cool 2-stage cooling system and an immersion heater controlled by a rheostat.

The reactor effluent passed through a six-port valve that allowed chemical analysis by either a gas chromatograph (Carle 8700) or

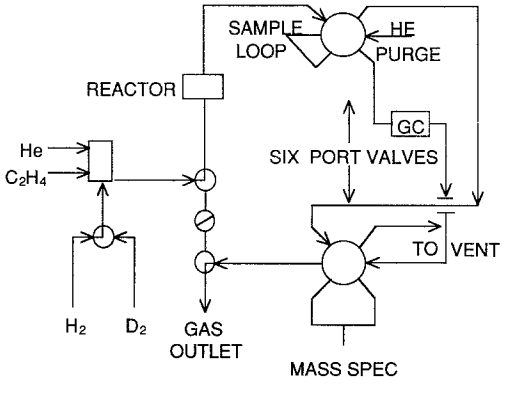

FIG. 1. Experimental apparatus for deuterium tracing experiments.

a mass spectrometer (EAI Quad 250B). The reactor effluent could be directed from the gas chromatograph to a six-port valve that allowed the separated gases to be analyzed by the mass spectrometer. The gas chromatograph was equipped with a 6-ft Poropak Q column operated at 350 K which allowed sampling at 3-min intervals.

The 0.04 wt% Pt/silica catalyst used in our previous steady state studies (*7*) was employed in these deuterium tracing studies. The platinum dispersion of this sample was equal to 1.0; however, ethylene hydrogenation is not a structure-sensitive reaction (e.g., Ref. (*7*)), and the choice of catalyst is, therefore, not critical. The amount of catalyst was adjusted to maintain ethylene conversions with deuterium typically between 1 and 5%. Prior to each experiment, the catalyst was treated in hydrogen at 573 K for 1 h. The apparatus was then evacuated, and the catalyst was cooled under flowing helium to the desired reaction temperature. Hydrogen and ethylene were introduced into the system and the catalyst was allowed to reach steady-state activity (ca. 20 min). Hydrogen was then replaced with deuterium at the same flow rate. Catalytic activity was observed to decrease as a result of the isotope effect. After steady state activity was again reached under these new conditions (ca. 15 min), isotopic analysis of the reactor effluent was commenced using the mass spectrometer. We have not attempted in our analyses to discriminate between positional isomers of the various paritally deuterated hydrocarbons.

Prior to mass spectroscopic analysis, mass spectra (25–32 amu) were obtained of the background gases associated with the vacuum chamber and the carrier gas from the gas chromatograph. Mass spectra (25–32 amu) were then collected of the ethylene pulse from three consecutive gas chromatographic separations of the reactor effluent. The ethane pulse could not be analyzed in a similar manner because the amount of ethane produced was not sufficient to be analyzed accurately.

Following analysis of the deuterium distribution in ethylene, mass spectroscopic analysis was conducted directly on the reactor effluent. This analysis included ethylene and ethane (25–36 amu) and the hydrogen isotopes (2–4 amu). The hydrocarbon analysis was conducted using an electron energy of 30 eV, whereas the hydrogen analysis was conducted using an electron energy of 15 eV, because the signal from helium interfered with the signal from deuterium. The electron energy of 15 eV is well below the 24 eV ionization potential of helium.

Effects on the mass spectroscopic data of molecular fragmentation and the presence of ^{13}C were corrected using an algorithm to deconvolute the different peaks in the spectra, based on a model developed by Lenz and Conner (*8, 9*). Analysis of the hydrogen isotopes was not complicated by fragmentation patterns. The sensitivity of the mass spectrometer to H_2 was 1.5 times the sensitivity to D_2. Zaera and Somorjai (*10*) found that the mass spectrometer sensitivity for H_2 was 1.7 times the sensitivity for D_2 at an electron energy of 70 eV. The sensitivity of HD with respect to H_2 was assumed to be 1.2 in the present study.

RESULTS

The experimental isotopic distributions for the deuteration of ethylene at sixteen different reaction conditions (temperatures from 248 to 333 K and D_2/C_2H_4 pressure ratios between 50 : 75 and 150 : 25 Torr) are shown in Table 1. The experimental errors in the ethane distributions were ±4 mol% for ethane-d_0 to ethane-d_2 and ±1 mol% for ethane-d_3 to ethane-d_6. The higher error associated with ethane-d_0 to ethane-d_2 was due to the overlap of ethylene in the mass spectra for these masses. Most of the chemistry extracted from these ethane deuterium distributions comes from ethane-d_1 and ethane-d_2, and to a lesser extent from ethane-d_0 and ethane-d_3. The relative amounts of ethane-(d_4–d_6) remain virtually unchanged despite changes in temperature or reactant pressures.

TABLE 1

Experimental Ethane Deuterium Distributions and M_4 for 0.04 wt% Pt/Cab-O-Sil1

C_2H_4 Pressure: (Torr)	75				25				10				25			
D_2 Pressure: (Torr)	50				50				50				150			
Temperature (K):	248	273	293	333	248	273	293	333	248	273	293	333	248	273	293	333
d_0 mol%	9	15	15	19	7	8	10	16	12	12	7	8	4	9	10	3
d_1 mol%	24	26	33	34	26	22	31	34	28	27	26	24	16	20	22	23
d_2 mol%	46	36	30	23	47	45	37	21	43	43	44	38	61	54	44	42
d_3 mol%	11	12	18	11	10	12	12	16	10	9	12	15	9	9	12	16
d_4 mol%	3	5	5	6	4	7	5	6	2	4	5	7	3	4	5	7
d_5 mol%	4	4	5	4	4	4	3	4	3	3	4	5	3	3	5	6
d_6 mol%	3	4	2	3	2	2	2	3	2	2	2	3	2	1	2	3
M_4	.006	.007	.004	.003	.025	.008	.008	.020	.069	.039	.035	.056	.013	.009	.018	.032

In contrast to ethane, the shape of the ethylene deuterium distributions did not change significantly at the different conditions. Measurable amounts of ethylene-d_4 were not detected, and ethylene-d_3 was present in only three experiments at concentrations less than 0.3% of the ethylene isotopic mixture. Ethylene containing two deuterium atoms was detected in most experiments at concentrations less than 1% and usually less than 0.5%. The average number of deuterium atoms incorporated into the ethylene is reported in Table 1 as M_4. These values depend on the amount of ethylene which had been converted to ethane, with higher values of M_4 observed at higher ethylene conversions.

Table 1 shows that increasing the reaction temperature leads to a decrease in the amount of ethane-d_2 and a broadening of the ethane deuterium distributions. Figure 2 shows this broadening with temperature at the reaction conditions of 25 Torr ethylene and 150 Torr deuterium. Furthermore, the ethane distribution shifts with changes in the D_2/C_2H_4 ratio. At a high D_2/C_2H_4 ratio (50 Torr D_2 and 10 Torr ethylene), the amounts of ethane-d_3 to ethane-d_6 increase at the expense of ethane-d_0 to ethane-d_2 with increasing temperature. At a lower D_2/C_2H_4 ratio (50 Torr D_2 and 75 Torr ethylene), the ethane deuterium distributions broaden as the temperature increases, with ethane-d_0 and ethane-d_1 increasing while ethane-d_2 decreases. In addition, the distribution maximum shifts from ethane-d_2 at lower temperatures to ethane-d_1 at temperatures above 293 K.

Table 1 also shows the effect of varying the ethylene pressure at a constant deuterium pressure of 50 Torr. At 248 K, the ethane distributions remain relatively unchanged as the ethylene pressure is increased from 10 to 75 Torr. At 293 K, the amounts of ethane-d_0 and ethane-d_1 increase at the expense of ethane-d_2 as the ethylene pressure increases. In addition, the distribu-

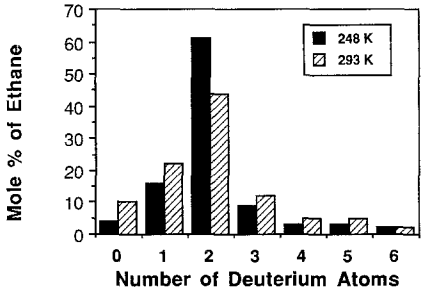

FIG. 2. Experimental ethane isotopic distributions resulting from reaction of 150 Torr deuterium with 25 Torr ethylene at 248 and 293 K.

tion maximum shifts from ethane-d_2 to ethane-d_1 as the ethylene pressure increases from 25 to 75 Torr.

At all temperatures, the ethane distributions narrow around ethane-d_2 as the deuterium pressure increases. Table 1 shows that at 25 Torr ethylene the amount of ethane-d_1 decreases and ethane-d_2 increases as the deuterium pressure increases from 50 to 150 Torr. This change is more pronounced at 333 K, where the distribution maximum changes from ethane-d_1 to ethane-d_2 as the deuterium pressure increases.

RESULTS OF KINETIC ANALYSES

The results of previous deuterium tracing studies have been adequately explained in terms of the relative rates of the elementary steps of the competitive Horiuti–Polanyi mechanism (*3, 5, 11–13*). These earlier analyses, however, did not incorporate the results of steady-state kinetic studies. As described below, we now attempt to describe consistently the results of our deuterium tracing studies and our steady-state kinetic studies (*7*). In addition, we have reconciled elsewhere (*1*) the steady-state kinetic results with the temperature programmed desorption and reaction studies of co-adsorbed ethylene and hydrogen on Pt single crystals observed by Berlowitz *et al.* (*14*).

The steady-state kinetic results (*7*) showed that the ethylene order was zero at ethylene pressures above 75 Torr and it was slightly negative at lower ethylene pressure and higher reaction temperatures. These results suggest that hydrocarbon species are the most abundant reactive intermediates on the catalyst surface and that hydrogen competes with ethylene for adsorption on active sites at higher temperatures and lower ethylene pressure. The observed half-order kinetics with respect to hydrogen pressure at lower temperatures suggest that hydrogen adsorption is equilibrated at these conditions. The change in the hydrogen kinetic order with temperature suggests a change in the nature of the slow steps in the reaction mechanism. The breadth of the deuterium distribution in ethane suggests that at least one of the surface hydrogenation steps is reversible, while the relatively high amounts of ethane-d_0 and ethane-d_1 indicate that the hydrogen adsorptive/desorptive step is not very fast. The modified Horiuti–Polanyi mechanism shown below was found to describe the observed experimental results (*1*).

1. $H_2 + 2S \leftrightarrow 2HS$
   Noncompetitive hydrogen adsorption
2. $HS + S' \leftrightarrow HS' + S$
   Noncompetitive hydrogen activation
3. $C_2H_4 + 2^* \leftrightarrow {}^*C_2H_4^*$
   Ethylene adsorption
4. ${}^*C_2H_4^* + HS' \leftrightarrow {}^*C_2H_5^* + S'$
   Initial hydrogenation
5. ${}^*C_2H_5^* + HS' \leftrightarrow C_2H_6 + 2^* + S'$
   Second hydrogenation
6. $H_2 + 2^* \leftrightarrow 2H^*$
   Competitive hydrogen adsorption
7. $H^* + S' \leftrightarrow HS' + ^*$
   Competitive hydrogen activation.

In this mechanism, ethylene adsorbs associatively and occupies two surface sites. Hydrogen can adsorb dissociatively either on surface sites (*) in competition with ethylene or on noncompetitive adsorption sites (S). Hydrogen adsorbed competitively (H*) and noncompetitively (HS) can be converted to surface hydrogen (HS′) that can subsequently react with adsorbed hydrocarbon species. The associatively adsorbed ethylene reacts with HS′ to produce an adsorbed surface ethyl species, which from geometric considerations is expected to occupy two sites.

The noncompetitive S-sites adsorb hydrogen but are inaccessible to hydrocarbon molecules. At low temperatures, the adsorption of hydrogen on S-sites is equilibrated and half-order hydrogen kinetics are observed. At higher temperatures and lower ethylene pressures, more surface sites (*) become available for hydrogen adsorption, and the reaction shifts to a more conventional competitive pathway where first-order hydrogen kinetics are observed. This

mechanism involves an activation step for the adsorption of hydrogen, since analyses of the competitive and noncompetitive mechanisms without hydrogen activation predict ethane deuterium distributions that have less ethane-d_0 and ethane-d_1 than observed experimentally. This difference is due to H atoms placed on the surface by dehydrogenation of the ethyl species, which leave the surface as HD instead of reacting with adsorbed hydrocarbon species to form ethane-d_0 and ethane-d_1. Sato and Miyahara (*12*) suggested a similar hydrogen activation step on the surface to explain the results of the reaction of H_2, D_2, C_2H_4, and C_2D_4 over nickel.

Kinetic analysis of the steady state kinetic results using the above Horiuti–Polanyi mechanism requires the simultaneous solution of five surface steady-state equations for reactive adsorbed species and the three site balances for catalyst surface sites. Kinetic analysis of the deuterium distributions requires the solution of the material balances equations for 15 isotopic gas-phase and 17 isotopic surface species. The following 15 isotopic gas phase species can be observed from the reaction of D_2 with C_2H_4:

H_2	HD	D_2	
C_2H_4	C_2H_3D	$C_2H_2D_2$	C_2HD_3
C_2D_4			
C_2H_6	C_2H_5D	$C_2H_4D_2$	$C_2H_3D_3$
$C_2H_2D_4$	C_2HD_5	C_2D_6.	

We define g_{ij} as the fraction of a particular gaseous species that consists of i H-atoms and j D-atoms. The above 15 isotopic species can be used to define the following 15 measurable g_{ij} variables:

g_{20}	g_{11}	g_{02}	
g_{40}	g_{31}	g_{22}	g_{13}
g_{04}			
g_{60}	g_{51}	g_{42}	g_{33}
g_{24}	g_{15}	g_{06}.	

These quantities must satisfy the appropriate normalization conditions that $\Sigma g_{ij} = 1$ for each chemical species (H_2, C_2H_4, and C_2H_6).

In addition to the gas-phase species, the concentrations of the following 17 surface isotopic species must be considered:

HS	DS	
HS′	DS′	
H*	D*	
$*C_2H_4^*$	$*C_2H_3D^*$	$*C_2H_2D_2^*$
$*C_2HD_3^*$	$*C_2D_4^*$	
$*C_2H_5^*$	$*C_2H_4D^*$	$*C_2H_3D_2^*$
$*C_2H_2D_3^*$	$*C_2H_1D_4^*$	$*C_2D_5^*$

As above, we define f_{ij} as the fraction of a particular surface species that consists of iH-atoms and j D-atoms. The above 17 isotopic surface species can be used to define the following 17 f_{ij} variables,

f_{s10}	f_{s01}	
$f_{s'10}$	$f_{s'01}$	
f_{m10}	f_{m01}	
f_{40}	f_{31}	f_{22}
f_{13}	f_{04}	
f_{50}	f_{41}	f_{32}
f_{23}	f_{14}	f_{05},

which satisfy the appropriate normalization conditions that $\Sigma f_{ij} = 1$ for each surface species (HS, HS′, H*, $*C_2H_4^*$, and $*C_2H_5^*$).

Material balance equations are written to relate the different gaseous species to rates, R_i, of the various steps in the modified Horiuti–Polanyi mechanism. The forms of these equations for C_2H_3D, HD, and $C_2H_4D_2$ are shown below,

$$\frac{d(F_{C_2H_4}g_{31})}{dt} = 0$$

$$= F^0_{C_2H_4}g^0_{31} - F_{C_2H_4}g_{31} - R_3\,g_{31} + R_{-3}f_{31}$$

$$\frac{d(F_{H_2}g_{11})}{dt} = 0 = F^0_{H_2}g^0_{11} - F_{H_2}g_{11}$$

$$- (R_1 + R_6)g_{11} + 2R_{-1}(f_{s10}f_{s01}) + 2R_{-6}(f_{m10}f_{m01})$$

$$\frac{d(F_{C_2H_6}g_{42})}{dt} = 0 = F^{o}_{C_2H_6}g^{o}_{42} - F_{C_2H_6}g_{42} + R_5(f_{32}f_{s'10} + f_{41}f_{s'01}),$$

where F_i^o and F_i are the molecular flow rates per active site for species i at the inlet and outlet of the catalyst bed, respectively. The fraction of reactor inlet consisting of a gas phase isotopic species is given by g_{ij}^o. The forward and reverse reaction rate of the elementary steps are designated by R_i and R_{-i}, respectively, and these rates have units of molecules reacted per site per second.

Material balances are also written for all surface species, as shown below for adsorbed $*C_2H_2D_2^*$, $*C_2H_3D_2^*$, HS, H*, and HS',

$$\frac{d(\theta_1 f_{22})}{dt} = 0 = R_3 g_{22} - R_{-3}f_{22} - R_4 f_{22} + R_{-4}\left(\frac{3}{5}f_{32} + \frac{3}{5}f_{23}\right)$$

$$\frac{d(\theta_2 f_{32})}{dt} = 0 = R_4(f_{22}f_{s'10} + f_{31}f_{s'01}) - R_{-4}f_{32} - R_5 f_{32}$$

$$\frac{d(\theta_3 f_{s10})}{dt} = 0 = R_1(2g_{20} + g_{11}) - 2R_{-1}(f_{s10}^2 + f_{s10}f_{s01}) - R_2 f_{s10} + R_{-2} f_{s'10}$$

$$\frac{d(\theta_4 f_{m10})}{dt} = 0 = R_6(2g_{20} + g_{11}) - 2R_{-6}(f_{m10}^2 + f_{m10}f_{m01}) - R_7 f_{m10} + R_{-7}f_{s'10}$$

$$\frac{d(\theta_5 f_{s'10})}{dt} = 0 = R_2 f_{s10} + R_7 f_{m10} - (R_{-2} + R_4 + R_5 + R_{-7})f_{s'10} + R_{-4}\left(f_{50} + \frac{4}{5}f_{41} + \frac{3}{5}f_{32} + \frac{2}{5}f_{23} + \frac{1}{5}f_{14}\right),$$

where θ_1 is the total surface coverage by all ethylene species, θ_2 is the total surface coverage by ethyl species, θ_3 is the total surface coverage by hydrogen species on the S sites, θ_4 is the total surface coverage by hydrogen species on the * sites, and θ_5 is the total surface coverage by the activated hydrogen.

It should be noted that for a rigorous analysis of the data, the experimentally measured isotope effect should be used to correct the various rates, R_i. In particular, each R_i in the above equations is an average rate for the various isotopic species. The distributions predicted with corrections for isotope effects, however, were different by at most 1–3% from those values predicted without consideration of isotope effects. These changes are mostly in ethane-d_0 to ethane-d_2, with ethane-d_0 and ethane-d_1 decreasing and ethane-d_2 increasing when the isotope effect is neglected.

A general regression analysis was performed to determine a consistent set of kinetic parameters, i.e., preexponential factors and activation energies for each step, that describes the results of steady state and deuterium tracing experiments. This analysis used a nonlinear equation solving routine for the 8 steady-state equations describing the total surface coverages and the 32 isotopic material balances discussed above. The general regression analysis then adjusted the kinetic parameters to minimize deviations in predicting the amounts of ethane-d_0 through ethane-d_3 and the steady state catalytic activity for each of the experimental reaction conditions studied. Table 2 shows values of the kinetic parameters that correctly describe the essential aspects of the deuterium tracing and steady state kinetic data.

It is important to note that the adjustment of kinetic parameters in this study was constrained to be consistent with surface science measurements for the adsorption/desorption of ethylene and hydrogen on platinum. In particular, the ethylene adsorption kinetic parameters were estimated using a sticking coefficient of 1.0 with no activation energy, as reported in the literature (*15, 16*). The kinetic parameters for the ethylene desorption steps were determined from temperature programmed desorption studies (*14, 17–19*). The kinetic parameters for hydrogen adsorption on platinum (step 6) were estimated using a sticking coefficient

TABLE 2

Kinetic Parameters of the Modified Horiuti–Polanyi Mechanism for the Hydrogenation of Ethylene on Platinum

Step	A_{for}	E_{for} (kcal/mol)	A_{rev}	E_{rev} (kcal/mol)
1	0.20	0.0	9.9×10^{9}	6.0
2	2.0×10^{11}	10.6	3.2×10^{9}	11.0
3	4.0×10^{5}	0.0	1.2×10^{7}	9.0
4	7.5×10^{9}	9.4	5.5×10^{12}	12.0
5	4.3×10^{11}	9.0	6.0×10^{4}	23.2
6	1.5×10^{5}	0.0	1.4×10^{9}	6.0
7	1.3×10^{11}	10.8	1.1×10^{13}	11.0

Note. Preexponential factors are in units of $Torr^{-1}\ s^{-1}$ for adsorption steps and s^{-1} for surface reactions and desorption steps.

of 0.1 with no activation energy, as reported in the literature (*20*). It is expected that kinetic parameters obtained at ultra high vacuum conditions are useful only in cases for which the surface regimes of the surface science measurements and the kinetic studies are similar. In addition, differences in crystallographic planes exposed on highly dispersed platinum particles compared to platinum single crystal surfaces are not expected to be important, since ethylene hydrogenation is not a structure-sensitive reaction. One important aspect of the analysis was the need to allow the rate constants for hydrogen desorption to be higher than those reported on clean surfaces (*20–23*). Since the steady-state surface is known to be highly covered by carbonaceous species, the increase in the rate constant may be attributed to the existence of interactions between adsorbed species. In fact, Salmerón and Somorjai (*24*) found that D_2 coadsorbed with ethylene on Pt(111) desorbs at substantially lower temperatures than on a clean Pt(111) surface at the same hydrogen coverage. The effects of the adsorbed hydrocarbon species are also evident in the present study from the low sticking coefficient required for the noncompetitive adsorption of hydrogen.

The number of S-sites used in the analysis was set at 0.3 times the number of competitive adsorption sites. This is an approximate number based on Monte Carlo simulations of the number of pair sites available for adsorption of dihydrogen on a Pt(111) surface saturated with hydrocarbon species. This number was found to have no effect on the steady-state kinetic analysis, provided that the preexponential factor for hydrogen adsorption was changed in such a manner as to compensate for the change in the number of S-sites. The number of S′-sites was arbitrarily set at 0.5 the number of competitive adsorption sites.

The kinetic parameters reported in Table 2 predict the proper steady state kinetic activities, shown in Fig. 3, and the proper trends for the ethane deuterium distributions, shown by comparison of Tables 1 and 3. Figure 3 shows the experimental (*7*) and predicted activities for ethylene hydrogenation over a range of hydrogen pressures from 50 to 650 Torr and a temperature range from 223 to 336 K at 25 Torr ethylene pressure. It can be seen that the kinetic analysis captures the proper variation in catalytic activity with hydrogen pressure and temperature. Table 3 demonstrates that the kinetic analysis shows the proper decrease in the amount of ethane-d_2 and the broadening of the ethane deuterium distributions with increasing temperature at all four sets of conditions. Table 3 also shows that at a large

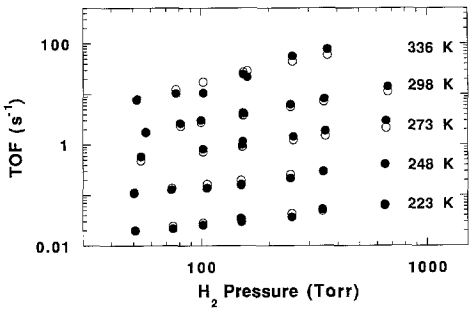

FIG. 3. Comparison of experimental (filled symbols) and predicted (open symbols) ethylene hydrogenation turnover frequencies versus hydrogen partial pressure. Experimental hydrogen kinetic orders are 0.47 at 223 K, 0.53 at 248 K, 0.66 at 273 K, 0.76 at 298 K, and 1.10 at 336 K.

D_2/C_2H_4 ratio (50 Torr D_2 and 10 Torr ethylene), the amounts of ethane-d_3 to ethane-d_6 increase at the expense of ethane-d_0 to ethane-d_2 with increasing temperature. At a lower D_2/C_2H_4 ratio (50 Torr D_2 and 75 Torr ethylene), the ethane deuterium distributions broaden as the temperature increases, with ethane-d_0 and ethane-d_1 increasing while ethane-d_2 decreases. In addition, Table 3 shows that the distribution maximum shifts from ethane-d_2 at lower temperatures to ethane-d_1 at temperatures above 293 K at 50 Torr D_2 and 75 Torr ethylene.

The kinetic analysis also predicts properly that the ethane distributions remain relatively unchanged as the ethylene pressure is changed from 10 to 75 Torr, at a deuterium pressure of 50 Torr and 248 K, as shown in Table 3. At 293 K, the distribution maximum shifts from ethane-d_2 to ethane-d_1 as the ethylene pressure increases from 25 Torr to 75 Torr. The proper trend with increasing deuterium pressure is also predicted. At all temperatures, the ethane distributions narrow around ethane-d_2 as the deuterium pressure increases. Table 3 shows that the amount of ethane-d_1 decreases and ethane-d_2 increases as the deuterium pressure increases from 50 to 150 Torr at 25 Torr ethylene.

DISCUSSION

Numerous deuterium tracing studies of ethylene hydrogenation, each conducted over a limited range of reaction conditions, have been reported in the literature (*5, 10–13, 25–29*). The trends shown in Table 1 are in general agreement with those observed by Bond (*26*) and Sato and Miyahara (*5*). Both of these previous investigations observed a broadening of the ethane deuterium distribution with increasing temperature. In addition, Bond observed on a Pt/silica catalyst that the yield of ethane-d_2 in-

TABLE 3

Predicted Ethane Deuterium Distributions and Values of M_4 from the Kinetic Parameters of Table 2

C_2H_4 Pressure: (Torr)	75				25				10				25			
D_2 Pressure: (Torr)	50				50				50				150			
Temperature (K):	248	273	293	333	248	273	293	333	248	273	293	333	248	273	293	333
d_0 mol%	6	10	15	29	5	8	11	15	4	6	7	7	3	4	5	6
d_1 mol%	30	35	38	41	29	32	34	35	27	29	29	27	23	27	28	26
d_2 mol%	46	37	31	22	48	40	35	31	50	43	40	35	56	48	43	38
d_3 mol%	14	13	12	7	14	15	14	14	15	16	17	19	15	16	17	19
d_4 mol%	3	4	3	1	3	4	5	5	4	5	6	9	3	4	6	8
d_5 mol%	1	1	1	0	1	1	1	1	1	1	1	3	0	1	1	3
d_6 mol%	0	0	0	0	0	0	0	0	0	0	0	0	0	0	0	0
M_4	.002	.003	.004	.003	.007	.011	.011	.013	.017	.026	.028	.039	.003	.006	.018	.008

TABLE 4

Predicted Rates of the Modified Horiuti–Polanyi Mechanism for the Reaction of Ethylene and Deuterium over Platinum Catalyst

C_2H_4 Pressure: (Torr)	75				25				10				25			
H_2 Pressure: (Torr)	50				50				50				150			
Temperature (K):	248	273	293	333	248	273	293	333	248	273	293	333	248	273	293	333
R_1	1.06	1.08	1.08	1.09	1.06	1.07	1.08	1.08	1.06	1.08	1.08	1.09	3.12	3.19	3.22	3.25
R_{-1}	0.96	0.71	0.39	0.06	0.95	0.71	0.40	0.08	0.95	0.72	0.42	0.11	2.94	2.52	1.81	0.52
R_2	0.22	0.76	1.45	2.72	0.22	0.75	1.46	3.08	0.21	0.75	1.47	3.49	0.37	1.39	3.01	7.59
R_{-2}	0.00	0.02	0.08	0.67	0.00	0.03	0.11	1.07	0.00	0.03	0.14	1.53	0.01	0.04	0.19	2.13
R_3	0.20	0.88	2.29	11.01	0.21	1.04	2.92	15.51	0.24	1.29	3.98	22.50	0.34	1.80	5.64	33.86
R_{-3}	0.07	0.39	1.20	7.71	0.07	0.39	1.20	7.67	0.07	0.38	1.19	7.60	0.07	0.38	1.19	7.56
R_4	0.25	1.40	4.28	24.93	0.28	1.66	5.55	39.59	0.31	2.04	7.37	56.30	0.43	2.72	9.85	77.87
R_{-4}	0.13	0.91	3.19	21.63	0.13	1.01	3.83	31.75	0.14	1.13	4.59	41.40	0.16	1.31	5.39	51.57
R_5	0.12	0.49	1.09	3.30	0.14	0.65	1.72	7.84	0.17	0.90	2.79	14.90	0.27	1.41	4.46	26.30
R_{-5}	0	0	0	0	0	0	0	0	0	0	0	0	0	0	0	0
R_6	0.05	0.22	0.57	2.75	0.16	0.78	2.19	11.63	0.45	2.41	7.46	42.18	0.77	4.04	12.70	76.19
R_{-6}	0.03	0.09	0.17	0.48	0.12	0.49	1.15	4.80	0.39	1.87	5.33	28.26	0.68	3.30	9.65	52.62
R_7	0.04	0.29	1.05	8.81	0.08	0.66	2.70	27.62	0.14	1.28	5.76	66.02	0.18	1.68	7.63	88.34
R_{-7}	0.00	0.04	0.24	4.26	0.05	0.09	0.61	13.97	0.01	0.20	1.52	38.19	0.01	0.20	1.53	41.20

creased with increasing D_2/C_2H_4 ratio at 273 K. An important innovation of the present study is to extract information about the rates, R_i, of the various hydrogenation processes over a wide range of conditions, allowing the variations in these rates with temperature and pressures to be tested for consistency with the results of steady-state kinetic studies conducted over the same catalyst and range of reaction conditions.

The elementary reaction rates presented in Table 4 were determined from the kinetic parameters of Table 2. The overall turnover frequency for ethylene hydrogenation is equal to the rate of step 5, which is irreversible. The ratio of the rate of an individual step i, to the overall rate is equal to R_i/R_5. In addition, the net rates (i.e., the forward rate minus the reverse rate) of steps 3 and 4 are equal to the turnover frequency. Furthermore, the overall turnover frequency is equal to the sum of the net rates of steps 1 and 6, where these net rates represent the contributions to the overall reaction of the noncompetitive and competitive pathways, respectively. The net rates of steps 2 and 7 are twice as large as the net rates of steps 1 and 6, respectively. It should be noted that these rates are reported for hydrogen (in contrast to deuterium), even when describing deuterium tracing results. Table 5 lists the reversibilities for each of the elementary steps as well as the percentage of the competitive pathway to the overall reaction rate.

A key finding of our steady state kinetic studies (*7*), was the increase in the value of the hydrogen reaction order with temperature. If the adsorption of hydrogen is equilibrated, then the observed rate should be half-order with respect to hydrogen; if this step is irreversible, then first order kinetics are expected. We observe in Table 5 that as the temperature increases from 248 to 333 K the reversibility decreases for the noncompetitive adsorption of hydrogen. For example, at 25 Torr ethylene and 150 Torr deuterium the reversibility of step 1 decreases from 11.6 to 0.1. In addition, Table 5 shows that as the temperature increases, the competitive nature of the production of ethane increases, and the kinetic orders thus reflect those of a competitive mechanism. For example, at 25 Torr ethylene and 50 Torr hydrogen the contribution from the competitive pathway increases from 28.6 to 87.1% as the temperature increases from 248 to 333 K. At low temperature, the surface is nearly saturated with hydrocarbon species,

TABLE 5

Reversibilities and Contribution of the Competitive Pathway for the Production of Ethane Predicted from the Rates Shown in Table 4

C_2H_4 Pressure: (Torr)	75				25				10				25			
H_2 Pressure: (Torr)	50				50				50				150			
Temperature (K):	248	273	293	333	248	273	293	333	248	273	293	333	248	273	293	333
Reversibilities																
R_1/R_5	8.8	2.2	1.0	0.3	7.6	1.6	0.6	0.1	6.2	1.2	0.4	0.1	11.6	2.3	0.7	0.1
R_2/R_5	0.9	0.8	0.7	0.4	0.8	0.6	0.4	0.2	0.6	0.4	0.3	0.1	0.7	0.5	0.3	0.1
R_3/R_5	1.7	1.8	2.1	3.3	1.5	1.6	1.7	2.0	1.4	1.4	1.4	1.5	1.3	1.3	1.3	1.3
R_4/R_5	2.1	2.9	3.9	7.6	2.0	2.6	3.2	5.0	1.8	2.3	2.6	3.8	1.6	1.9	2.2	3.0
R_6/R_5	0.4	0.4	0.5	0.8	1.1	1.2	1.3	1.5	2.6	2.7	2.7	2.8	2.9	2.9	2.8	2.9
R_7/R_5	0.2	0.3	0.5	1.3	0.3	0.5	0.8	1.8	0.4	0.7	1.0	2.2	0.3	0.6	0.9	1.7
% Competitive	16.7	26.5	36.7	68.8	28.6	44.6	60.5	87.1	35.3	60.0	76.3	93.4	33.3	52.5	68.4	89.6

thus allowing hydrogen to adsorb only on the noncompetitive adsorption sites. As the temperature increases, the surface coverage decreases and more competitive adsorption sites are available, increasing the rate of the competitive pathway.

The ethylene order becomes more negative as the reaction temperature increases, and the rate is nearly independent of ethylene pressure above 75 Torr (*7*). Table 5 shows that the competitive nature of the production of ethane increases with decreasing ethylene pressure. For example, the contribution from the competitive pathway increases from 26.5 to 60% as the ethylene pressure decreases from 75 to 10 Torr at 273 K. As the pressure of ethylene decreases, the surface coverage by carbonaceous species decreases, and the competitive pathway thus becomes more important.

The shape and extent of deuterium incorporation into ethane give information about the relative rates of the elementary steps. Table 6 shows the effects on the ethane deuterium numbers and M_4 of increasing the forward and reverse rates of each of the elementary steps, maintaining constant the net rates of each step. This table shows that an increase in the reversibility of step 4 decreases the amount of ethane-d_2 while increasing the amounts of the other ethane isotopic species. Accordingly, conditions that increase the reversibility of step 4 (e.g., increasing temperature or decreasing deuterium pressure) broaden the ethane deuterium distribution. This broadening is evident with increasing temperature for each of the four different pressure conditions shown in Table 1. Table 5 shows for each of these cases that the reversibility of step 4 increases with temperature. In addition, Table 1 shows a similar broadening as the deuterium pressure decreases from 150 to 50 Torr at an ethylene pressure of 25 Torr. In this case, Table 5 shows that the reversibility of step 4 increases from 3.0 to 5.0 with a decrease in deuterium pressure from 150 to 50 Torr at 333 K.

Table 5 shows that the shift in the distribution maximum from ethane-d_2 to ethane-d_1 is due to conditions where step 4 is highly reversible and the steps involving surface hydrogen are somewhat irreversible, e.g., increasing ethylene pressure and temperature. For example, Table 1 shows a shift in the distribution maximum from ethane-d_2 to ethane-d_1 at 333 K when the deuterium pressure decreases from 150 to 50 Torr; and, in this case, the reversibility of step 4 increases from 3.0 to 5.0 while the hydrogen activation

TABLE 6

Response of Ethane Distributions and Value of M_4 to an Increase in Reversibility of Specific Steps (R_i/R_5)

Step	d_0	d_1	d_2	d_3	d_4	d_5	d_6	M_4
1	−	−	+	+	+	+	+	+
2	−	−	+	+	+	+	+	+
3	+	+	+	−	−	−	−	+
4	+	+	−	+	+	+	+	+
6	−	−	+	+	+	+	+	+
7	−	−	+	+	+	+	+	+

steps (steps 2 and 7) remain relatively irreversible. A similar shift in the distribution maximum is noted at the lower D_2/C_2H_4 ratios with increasing temperature, e.g., 75 Torr ethylene and 50 Torr hydrogen. Table 5 shows at these conditions that the reversibility of step 4 increases from 2.1 to 7.6, while the hydrogen activation steps remain relatively irreversible as the temperature increases from 248 to 333 K.

The combined results of the steady state and deuterium tracing studies suggest the importance of hydrogen activation steps. The half-order hydrogen kinetics observed at lower temperatures suggest an equilibrated hydrogen adsorption step. However, Table 6 shows that a highly reversible hydrogen adsorption step produces small amounts of ethane-d_0 and ethane-d_1. The relatively large amounts of ethane-d_0 and ethane-d_1 shown in Table 1, therefore, suggest an irreversible hydrogen step. Accordingly, a rather irreversible hydrogen activation step is necessary to transform adsorbed atomic hydrogen to reactive atomic hydrogen. Similar reasoning suggests that the activation of competitively adsorbed hydrogen is also important. These results illustrate the key aspect of combining the results of diverse experiments to develop a unified description of the essential surface chemistry involved in ethylene hydrogenation over platinum.

SUMMARY

The results of steady state and deuterium tracing studies suggest the importance of hydrogen activation steps. Specifically, the half-order hydrogen kinetics at lower temperatures require an equilibrated hydrogen adsorption step; however, the relatively large amounts of ethane-d_0 and ethane-d_1 suggest a slow hydrogen step. Accordingly, a rather irreversible hydrogen activation step is necessary to transform the adsorbed atomic hydrogen to a more reactive form.

A key aspect of the present paper is that the kinetic information contained in the deuterium tracing results has been extracted by an analysis that incorporates results from steady state kinetic studies and information from the surface science literature (e.g., Ref. (*1*)). This kinetic analysis of diverse experimental data from ethylene hydrogenation on platinum was based on a modified Horiuti–Polanyi mechanism that includes competitive and noncompetitive hydrogen adsorption pathways, each modified by a hydrogen activation step. The steady state kinetic results provide information regarding the relative rates of hydrogen adsorption and ethane formation steps. Deuterium tracing provides complementary information about these steps, as well as vital information about the rates of hydrogen exchange on the surface between adsorbed ethylene and ethyl species, and the activation of hydrogen from competitive and noncompetitive adsorption sites to reactive sites.

In closing, we note that analysis of kinetic data of a given type alone is not generally sufficient to establish a thorough description of the surface chemistry. In contrast, we suggest that microkinetic analysis of diverse

experimental data from such measurements as steady-state kinetics, isotopic tracing, and temperature programmed desorption provides a more detailed description of the essential surface chemistry involved in the catalytic process than does analysis of experimental data from a single type of measurement.

ACKNOWLEDGMENTS

We acknowledge financial support from the National Science Foundation. We thank Jim Rekoske and Sanjay B. Sharma for their assistance with this work, Professor W. E. Stewart for providing us with his general regression analysis software (GREG), and Rod Bain for providing us with his equation solver (NNES).

REFERENCES

1. Rekoske, J. E., Cortright, R. D., Goddard, S. A., Sharma, S. B., and Dumesic, J. A., *J. Phys. Chem.* **96,** 1880 (1992).
2. Ozaki, A., Ed., "Isotopic Studies of Heterogeneous Catalysis," p. 238. Academic Press, New York, 1977.
3. Kemball, C., *J. Chem. Soc.*, 735 (1956).
4. Horiuti, J., and Polanyi, M., *Trans. Faraday Soc.*, **30,** 1164 (1934).
5. Sato, S., and Miyahara, K., *J. Res. Inst. Catal. Hokkaido Univ.* **23,** 1 (1975).
6. Happel, J., Ed., "Isotopic Assessment of Heterogeneous Catalysis," p. 196. Academic Press, Orlando, 1986.
7. Cortright, R. D., Goddard, S. A., Rekoske, J. E., and Dumesic, J. A., *J. Catal.* **127,** 342 (1991).
8. Lenz, D. H., and W. C. Conner, J., *Anal. Chim. Acta.* **173,** 227 (1985).
9. Lenz, D. H., Ph.D. Thesis, University of Massachusetts, 1986.
10. Zaera, F., and Somorjai, G. A., *J. Am. Chem. Soc.* **106,** 2288 (1984).
11. Bond, G. C., Phillipson, J. J., Wells, P. B., and Winterbottom, J. M., *Trans. Faraday Soc.* **60,** 1847 (1964).
12. Sato, S., and Miyahara, K., *J. Res. Inst. Catal. Hokkaido Univ.* **22,** 172 (1974).
13. Sato, S., and Miyahara, K., *J. Res. Inst. Catal. Hokkaido Univ.* **23,** 17 (1975).
14. Berlowitz, P., Megiris, C., Butt, J. B., and Kung, H. H., *Langmuir* **1**(2), 206 (1985).
15. Smith, D. L., and Merrill, R. P., *J. Chem. Phys.* **52,** 3588 (1970).
16. Weinberg, W. H., Deans, H. A., and Merrill, R. P., *Surf. Sci.* **41,** 312 (1974).
17. Godbey, D., Zaera, F., Yeates, R., and Somorjai, G. A., *Surf. Sci.* **167,** 150 (1986).
18. Windham, R. G., Bartram, M. E., and Koel, B. E., *J. Phys. Chem.* **92,** 2862 (1988).
19. Windham, R. G., and Koel, B. E., *J. Phys. Chem.* **94,** 1489 (1990).
20. Christmann, K., Ertl, G., and Pignet, T., *Surf. Sci.* **54,** 365 (1976).
21. Lu, K. E., and Rye, R. R., *J. Vacuum Sci. Technol.* **12,** 334 (1975).
22. McCabe, R. W., and Schmidt, L. D., *Surf. Sci.* **60,** 85 (1976).
23. Poelsema, B., Mechtersheimer, G., and Comsa, G., *Surf. Sci.* **111,** 519 (1981).
24. Salmerón, M., and Somorjai, G. A., *J. Phys. Chem.* **86,** 341 (1982).
25. Horiuti, J., and Miyahara, K., "Hydrogenation of Ethylene on Metallic Catalysts," *in* NBS-NSRDS No. 13. National Bureau of Standards, Washington, DC, 1968.
26. Bond, G. C., *Trans. Faraday Soc.* **52,** 1235 (1956).
27. Kazanskii, V. B., and Strunin, V. P., *Kinet. Catal. Engl. Trans.* **1,** 517 (1960).
28. Farkas, A., and Farkas, L., *J. Am. Chem. Soc.* **60,** 22 (1938).
29. Briggs, D., Dewing, J., Burden, A. G., Moyes, R. B., and Wells, P. B., *J. Catal.* **65,** 31 (1980).